

Optical Engineering

OpticalEngineering.SPIEDigitalLibrary.org

Design and analysis of seven-core photonic crystal fiber for high-power visible supercontinuum generation

Xue Qi
Sheng-Ping Chen
Ai-Jun Jin
Tong Liu
Jing Hou

Design and analysis of seven-core photonic crystal fiber for high-power visible supercontinuum generation

Xue Qi, Sheng-Ping Chen,* Ai-Jun Jin, Tong Liu, and Jing Hou

National University of Defense Technology, College of Optoelectronic Science and Engineering, No. 137, Yanwachi Street, Changsha, Hunan 410073, China

Abstract. We design a seven-core photonic crystal fiber with specifically designed dispersion and group velocity profile which is optimized for high-power visible supercontinuum (SC) generation pumped by $\sim 1\text{-}\mu\text{m}$ pulsed lasers. The fiber has both a large air-filling fraction and a large effective mode field area. Additionally, the in-phase supermode of this fiber exhibits an even field distribution after mode modification. The simulation results suggest that it has a great potential to generate a high-power SC extending to 400 nm, which is highly desirable in biological applications. © The Authors. Published by SPIE under a Creative Commons Attribution 3.0 Unported License. Distribution or reproduction of this work in whole or in part requires full attribution of the original publication, including its DOI. [DOI: [10.1117/1.OE.54.6.066102](https://doi.org/10.1117/1.OE.54.6.066102)]

Keywords: seven-core photonic crystal fiber; visible supercontinuum; high power.

Paper 150174 received Feb. 6, 2015; accepted for publication May 19, 2015; published online Jun. 18, 2015.

1 Introduction

Photonic crystal fibers (PCFs) applied for broadband supercontinuum (SC) generation have achieved great success.¹⁻⁴ However, the development of a high-power SC based on single-core PCF is restricted by its small mode field area because a large core size always leads to a dispersion mismatch with the $1\text{-}\mu\text{m}$ laser which is the most commonly used pump source for high-power all-fiber integrated SC generation.^{5,6} The power scaling ability and the extension of the spectrum is an apparent contradiction for single-core PCFs. Multicore PCFs offer a possibility of scaling up the mode field area to a large extent without a remarkable change in dispersion properties which show great potential in high-power supercontinuum generation.^{7,8} As shown in Ref. 7, 5.4-W SC spanning from 500 to 1700 nm was generated using a high-power femtosecond fiber amplifier with a central wavelength of 1038 nm and a seven-core nonlinear PCF with an air-filling fraction 0.55 where each core diameter was $3.8\ \mu\text{m}$ and there was a zero dispersion wavelength (ZDW) of the in-phase supermode 1025 nm. In Ref. 8, 64-W SC spanning from 500 to 1700 nm was demonstrated in a double cladding seven-core PCF with an air-filling fraction 0.6 where each core diameter was $3.5\ \mu\text{m}$ and there was a ZDW of the in-phase supermode 930 nm by using a high-power picosecond fiber laser with a central wavelength of 1064 nm. To date, the spectra of SC based on seven-core PCFs have not extended to 400 nm and the power fraction of the visible wavelengths is very low. However, the ultraviolet-blue region of the SC spectrum is highly desirable in biological applications, e.g., hyperspectral fluorescence lifetime imaging,⁹ optical coherence tomography,¹⁰ fluorescence microscopy,¹¹ and so on.

In this paper, we first analyze the physical mechanism of the “trapping effect” which dominates visible SC generation and demonstrates the limitation of the high-power visible SC generation based on existing seven-core PCFs. Then we utilize the method of altering the PCF structure to modify the

group-velocity profile and obtain suitable structural parameters for the seven-core PCF. In addition, we optimize the structural parameters for an even field distribution of the in-phase supermode of the seven-core PCF. Then we calculate the dispersion curve and group-velocity profile of the newly designed seven-core PCF. Finally, we simulate the SC generation with the newly designed seven-core PCF. The simulation results show that the newly designed seven-core PCF has a great potential as the primary nonlinear medium for high-power visible SC generation.

2 Design of Seven-Core Photonic Crystal Fiber

2.1 Design Principle

Visible SC generation using a 1064 nm ps pump source can be achieved using a PCF with a specifically designed dispersion and group-velocity profile.¹² The physical mechanism is shown as follows. First, the ps pump pulses are broken up into solitons no longer than ~ 100 fs due to modulation instability when pumping at a wavelength with anomalous dispersion but close to the ZDW of the PCF. While the solitons are formed from the pump pulses in the anomalous dispersion region, the solitons transfer energy into the normal dispersion region in the form of dispersive waves.¹³ Second, if the soliton duration is sufficiently short, the solitons can immediately start to red-shift due to intrapulse Raman scattering, also known as the soliton self-frequency shift.¹⁴ The dispersive waves initially have a lower group-velocity than the solitons and will lag behind the solitons. However, the solitons decrease their group-velocity as they gradually red-shift and eventually meet the dispersive waves.¹⁵ Third, the solitons and the dispersive waves experience a couple of interactive nonlinearity mechanisms due to their temporal overlap. One of the interactive nonlinearity mechanisms is the cross-phase modulation which leads to a blue-shift of the dispersive waves. The other is the four-wave mixing (FWM) which leads to the generation of energy at shorter wavelengths than the dispersive waves.¹⁶ The blue-shift mechanism can take place continuously as long as the

*Address all correspondence to: Sheng-Ping Chen, E-mail: chespn@163.com

solitons are able to red-shift. This process has been termed as the “trapping effect.”

With the mechanism described above, the maximum blue-shift is limited by the ability of the solitons to red-shift, while the red-shift is limited by the increase in both material loss and confinement loss at wavelengths of about $2.5 \mu\text{m}$ in the near-infrared. Therefore, we can predict the location of the blue edge of an SC spectrum for a fiber from the group-velocity profile when the fiber has an anomalous dispersion region extending far into the near-infrared.¹⁵

2.2 Structural Parameters

As discussed in Sec. 2.1, the group-velocity-matched blue-edge (matched to $2.5 \mu\text{m}$) of the previously used seven-core PCFs all extend above 500 nm . They are obviously not suitable to generate the blue-extended SC. To overcome this drawback, we design a seven-core PCF with the ZDW shorter than and closer to the pump wavelength and the group-velocity-matched blue-edge below 400 nm . Here, we consider the pump wavelength as 1064 nm because the lasers with this wavelength have achieved considerable progress. The fibers’ group-velocity profile generally shows an inverted “U” shape. The material dispersion provides the dominant contribution to the total dispersion at short wavelengths, while the waveguide dispersion provides the dominant contribution to the total dispersion at long wavelengths.

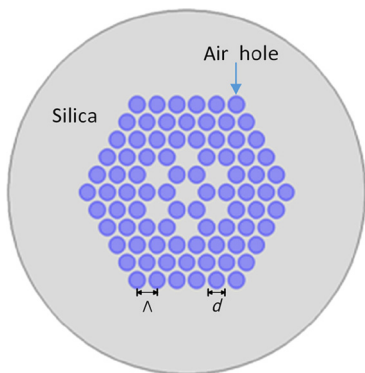


Fig. 1 Seven-core photonic crystal fiber. Blue areas denote air holes, while gray areas denote silica glass.

That is to say, either modifying the PCF structure or directly altering the PCF material can shift the group-velocity profile. In this paper, we consider a steeper decrease at infrared wavelengths in the group-velocity profile by modifying the PCF structure.

The model of the seven-core PCF is shown in Fig. 1. In the cladding, five rings of air holes with diameter d are arranged in a hexagonal pattern. Six air holes in the second ring are substituted by six solid-core rods forming the seven-core PCF and each core has a diameter of d_{core} which equals to $2\Lambda - d$. The distance between adjacent air holes’ centers is pitch Λ and the air-filling fraction is defined as d/Λ . The dispersion and group-velocity discussed below are of the in-phase supermode of the seven-core PCF which has the preferable Gaussian-like far-field intensity distribution.

In our analysis, we use a fully vectorial approach employing the finite element method based on edge/nodal hybrid elements and anisotropic perfectly matched layer boundary conditions. Simulations are carried out using the commercially available COMSOL Multiphysics software. The spectral dependence of the refractive index for silica is calculated from the simpler form of the Sellmeier equation¹⁷ and is taken into account in the simulations. The effective refractive indices and electric field distributions at wavelengths from 0.3 to $2.6 \mu\text{m}$ are obtained. Chromatic dispersion and the effective mode field area are calculated.

In Figs. 2(a) and 2(b), we plot the calculated dispersion curves and group-velocity profiles of seven-core PCF for structures with fixed $d_{\text{core}} = 4.5 \mu\text{m}$ and various values of d/Λ between 0.45 and 0.8 . Figure 2(a) reveals a gradual shift of the zero dispersion point toward shorter wavelengths, and in Fig. 2(b), there is a steeper decrease at infrared wavelengths in the group-velocity profile for seven-core PCFs with gradually increasing air-filling fractions, but with constant diameters of the cores. This change is similar to the case of a single-core PCF as stated in Ref. 12. However, in the simulation, we also find that a too large air-filling fraction results in a mode field distribution similar to single-core PCF at a short wavelength. The explanation is probably that a larger air-filling fraction leads to a stronger confinement of the optical field at short wavelengths to the fiber core. Then the evanescent field could hardly couple and supermodes cannot form.

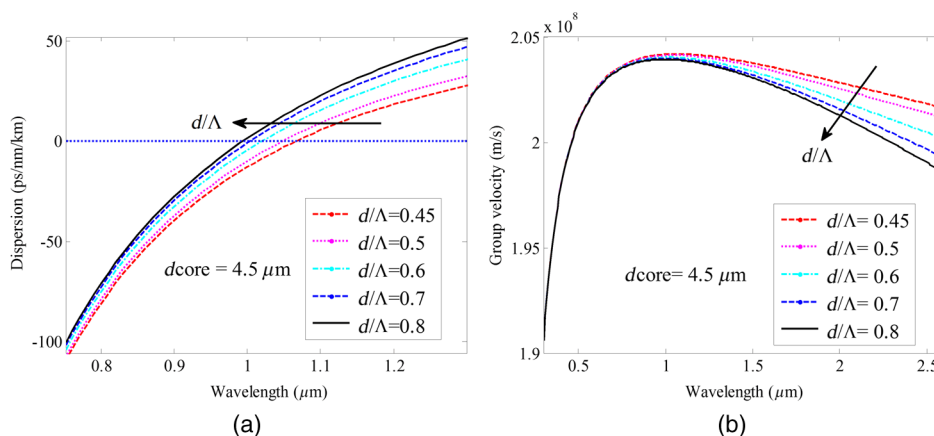


Fig. 2 Calculated spectral dependence of (a) dispersion and (b) group-velocity of seven-core photonic crystal fiber (PCF) for gradually increasing d/Λ from 0.45 to 0.8 with fixed $d_{\text{core}} = 4.5 \mu\text{m}$.

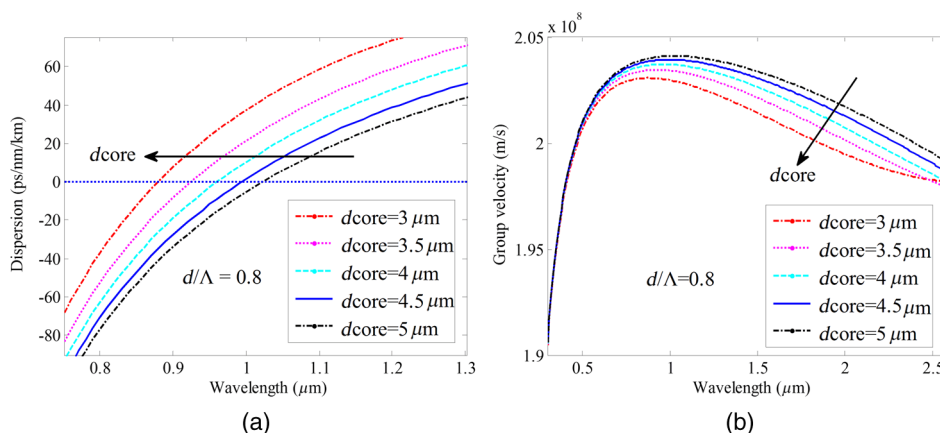


Fig. 3 Calculated spectral dependence of (a) dispersion and (b) group-velocity of seven-core PCF for gradually increasing d_{core} from 3 to 5 μm with fixed $d/\Lambda = 0.8$.

In Figs. 3(a) and 3(b), we plot the calculated dispersion curves and group-velocity profiles of a seven-core PCF for structures with fixed $d/\Lambda = 0.8$ and various values of the d_{core} in the range of 3 to 5 μm . The graph in Fig. 3(a) reveals a gradual shift of the zero dispersion point toward shorter wavelengths, and in Fig. 3(b), there is a steeper decrease at infrared wavelengths in the group-velocity profile for seven-core PCFs with gradually decreasing core diameters, but constant air-filling fractions. This change is similar to the case of a single-core PCF as stated in Refs. 18 and 19. The steeper decrease at infrared wavelengths in the group-velocity profile means a deeper blue SC spectrum. However, the decrease of the core diameter shifts the ZDW further away from the pump wavelength and results in a significant decrease in the visible spectrum.¹²

Hence, we choose the structure with $d/\Lambda = 0.8$ and $d_{\text{core}} = 4.5 \mu\text{m}$ to balance the ZDW and the decrease at infrared wavelengths in the group-velocity profile to balance the power and the spectral extendibility of visible SCs. The ZDW of this structure is 994 nm and the group-velocity-matched blue-edge (matched to 2.5 μm) is 430 nm. Though the blue-edge is not below 400 nm, experiments in Refs. 12 and 15 showed that there was a mismatch between the predicted group-velocity profile and the experimental results. Specifically, in experiments the spectrum could be more blue-shifted, possibly because FWM can occur between the soliton and the dispersive wave leading to the generation of energy at wavelengths shorter than

the dispersion wave.¹⁶ The simulation results of ZDW and the group-velocity-matched blue-edge with changing d/Λ and d_{core} are summarized in Table 1.

2.3 Mode Modification

Optical field propagates in the core region of the seven-core PCF in the form of seven supermodes by evanescent field interaction in the weak coupling approximation.²⁰ Only the in-phase supermode, where all cores have the same phase, has the preferable Gaussian-like far-field intensity distribution. In Fig. 4(a), we plot the field distribution of the in-phase supermode of the designed seven-core PCF. The field distribution is obviously not even and the central core has more power than the surrounding six cores. The reason is probably that the central core couples with the surrounding six cores while the surrounding six cores only couple with three adjacent cores because we have supposed that only adjacent cores couple with each other in the weak coupling approximation. By resolving the coupled-mode equation,²¹ the power of the central core is $(\sqrt{7} - 1)^2 = 2.71$ times that of the surrounding six cores.

We can modify the inner six air holes' diameters²¹ to change the area of the cores or modify the material of the cores to change their refractive index to alter the self-coupling and cross-coupling coefficients of the seven cores and get an even field distribution of the in-phase supermode, as shown in Fig. 4(b). Here, the diameter of the six air holes in the inner ring is changed from 3 to 3.003 μm .

Table 1 Simulation results of ZDW and group-velocity-matched blue-edge (matched to 2.5 μm) with changing d/Λ and d_{core} .

$d_{\text{core}} = 4.5 \mu\text{m}$	d/Λ	ZDW (nm)	Blue-edge corresponding to 2.5 μm (nm)	$d/\Lambda = 0.8$		
				$d_{\text{core}} (\mu\text{m})$	ZDW (nm)	Blue-edge corresponding to 2.5 μm (nm)
	0.45	1066	547	5	1023	443
	0.5	1049	521	4.5	994	430
	0.6	1021	478	4	960	417
	0.7	1004	449	3.5	924	410
	0.8	994	430	3	879	414

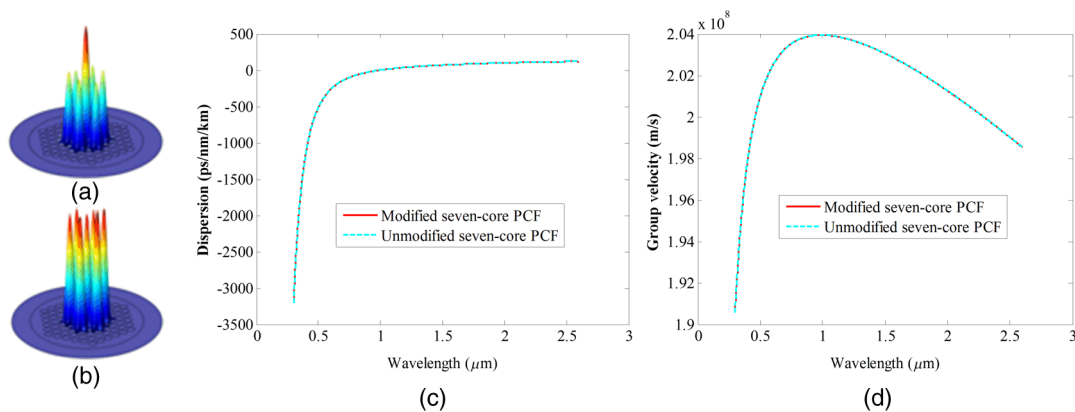


Fig. 4 Mode modification: (a) field distribution of unmodified and (b) modified seven-core PCF, (c) calculated spectral dependence of dispersion, and (d) group-velocity of the unmodified and the modified seven-core PCF.

In Figs. 4(c) and 4(d), we plot the dispersion curves and group-velocity profiles of the modified seven-core PCF with an even field distribution and the unmodified seven-core PCF with an uneven field distribution of the in-phase supermode, respectively. From Figs. 4(c) and 4(d), we can see that the tiny change of the diameter of the inner six air holes brings little change to the dispersion curve and group-velocity profile. As a result, the final structural parameters of our designed seven-core PCF are as follows: the air holes' pitch $\Lambda = 3.75 \mu\text{m}$, the diameter of the six air holes in the first ring $d_1 = 3.003 \mu\text{m}$ and the diameter of the other air holes $d_2 = 3 \mu\text{m}$. The air-filling fraction is $d/\Lambda = 0.8$, the central core diameter is $d_{\text{core1}} = 4.497 \mu\text{m}$ and the surrounding six cores' diameters are $d_{\text{core2}} = 4.5 \mu\text{m}$.

The newly designed seven-core PCF has a significantly larger effective mode field area compared with single-core PCFs. As seen in Fig. 5, at a wavelength of 1064 nm, the mode field area of the in-phase supermode of the designed seven-core PCF is $58 \mu\text{m}^2$ and the mode field diameter is $8.6 \mu\text{m}$, whereas the mode field area of SC-5.0-1040 made by NKT Photonics, which is a single-core PCF, is $12.78 \mu\text{m}^2$ and the mode field diameter is $4.8 \mu\text{m}$. In contrast to the single-core PCF, the designed seven-core PCF

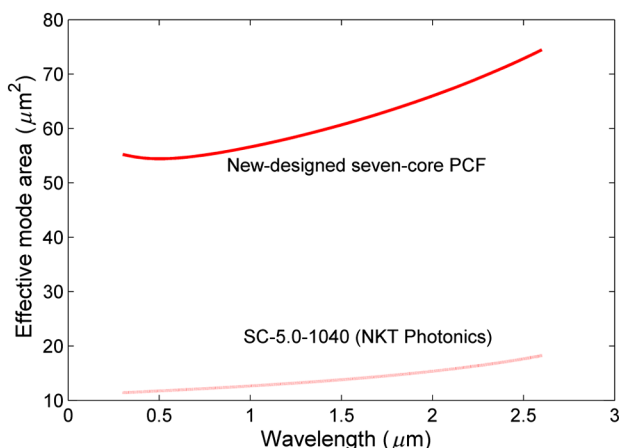


Fig. 5 Effective mode area as a function of wavelengths for the newly designed seven-core PCF and SC-5.0-1040 (NKT Photonics) [red line for newly designed seven-core PCF and red dotted line for SC-5.0-1040 (NKT Photonics)].

effectively increases the end facet damage threshold and decreases the mode field mismatch when spliced to the large mode area double cladding pigtail fiber of the pump laser. As a result, the newly-designed seven-core PCF has a great potential for upscaling the average power of the SC sources.

3 Supercontinuum Simulation and Discussion

SC generation in optical fibers is well described by the generalized nonlinear Schrodinger equation (GNLSE).¹⁷ We apply the electric field envelope A at a propagation distance z in a retarded reference time frame $T = t - \beta_1 z$ in the following form

$$\frac{\partial A}{\partial z} + \frac{\alpha}{2} A - \sum_{k \geq 2} \frac{i^{k+1}}{k!} \beta_k \frac{\partial^k A}{\partial T^k} = i\gamma \left(1 + i\tau_{\text{shock}} \frac{\partial}{\partial T} \right) \times (A(z, T) \int_{-\infty}^{\infty} R(T') |A(z, T - T')|^2 dT'), \quad (1)$$

where β_k is the k 'th order dispersion coefficient associated with the Taylor series expansion of the propagation constant $\beta(\omega)$ about the central frequency of the pump pulse, ω_0 ; α

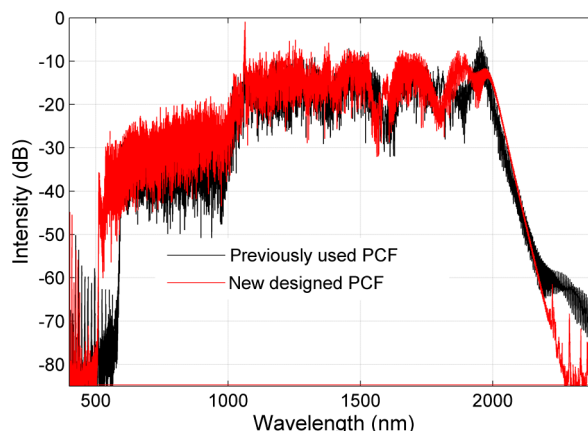


Fig. 6 Calculated SC spectra after 3 m of propagation in the newly designed and previously used seven-core PCF in Ref. 8 (red line for newly designed seven-core PCF and black line for previously used seven-core PCF in Ref. 8).

Table 2 Main parameters of the newly designed and the previously used seven-core PCF in Ref. 8.

	A_{eff} at 1064 nm	ZDW	Group-velocity-matched blue-edge (matched to 2.5 μm)	High-order dispersion		
				β_1	β_2	β_3
Unit	μm^2	nm	nm	ps/km	ps ² /km	ps ³ /km
Newly designed PCF	58.0	994	430	4.90×10^6	-9.45	8.33×10^{-2}
Previously used PCF in Ref. 8	39.3	962	516	4.91×10^6	-12.83	7.57×10^{-2}

is the fiber loss as a function of frequency; γ is the nonlinear coefficient defined by $\gamma = \omega_0 n_2 / (c A_{\text{eff}})$, where n_2 is the nonlinear refractive index given by $n_2 = 2 \times 10^{-20} \text{ m}^2 \text{ W}^{-1}$, ω_0 is the angular frequency of the optical carrier, c is the speed of light, and A_{eff} is the fiber's effective area. The form of the nonlinear response function $R(t)$ can be written as $R(t) = (1 - f_R)\delta(t) + f_R h_R(t)$, which includes both the instantaneous Kerr contribution and the delayed Raman response.

For the direct demonstration of the newly designed seven-core PCF, we simulate the SC spectra through the GNLS with the split-step Fourier method. Meanwhile, we give the simulation result with the previously used seven-core PCF in Ref. 8 for comparison as shown in Fig. 6. In our simulation, the parameters of the pump laser are identical, where the pump wavelength $\lambda_0 = 1.064 \mu\text{m}$, the peak power $P_0 = 15 \text{ kW}$, the FWHM $T_0 = 20 \text{ ps}$, and initial chirp $C = 0$. The fiber length of the two seven-core PCFs for the simulation is 3 m. The main differences between the two seven-core PCFs are shown in Table 2. Here, we just list β_1 to β_3 for simplicity, while in the simulation, β_1 to β_6 are all included.

As seen in Fig. 6, when the red-shift soliton locates at about 2000 nm, the blue-edge of the spectrum of the newly designed seven-core PCF can extend over 90 nm shorter than the previously used seven-core PCF in Ref. 8 due to the modified dispersion and group-velocity characteristics. Moreover, the intensity of the visible spectrum of the SC based on the newly designed PCF is obviously higher than the SC based on the previously used PCF. There is an approximately 10 dB increase in the visible spectrum because the ZDW of the proposed PCF is closer to the pump wavelength than the previously used PCF.

In our simulation, the spectrum of the previously used seven-core PCF in Ref. 8 is from 600 to 2000 nm but in the experiment in Ref. 8 it can extend to 500 nm. One possible explanation for this discrepancy could be that the red-shift soliton has not shifted to the long wavelength enough in the simulation because of low-peak power or the low-nonlinearity coefficient. However, the trend of extending a bluer edge of the SC spectrum by modifying the dispersion and the group-velocity is shown in the simulation. Therefore, we predict that the newly designed seven-core PCF can extend to an even shorter wavelength than the previously used PCF.

As the simulation indicates, the intensity of the optical field distribution is very sensitive to any alteration of hole size, e.g., from 3 to 3.003 μm . Obviously, to perfectly control the tolerance in the fabrication will be challenging. An industrial standard fiber drawing tower (such as the Nextrom

brand) can be used for capillary and fiber fabrication. The capillaries used to stack the hole structured preform can be carried out based on Heraeus F300 throughout. A typical capillary outer diameter is $1 \pm 0.001 \text{ mm}$. Fiber tolerance can be controlled within $\pm 0.5 \mu\text{m}$. Therefore, the overall tolerance is larger than the designed changes of the hole size. To push the fabrication tolerance even tighter might be one solution, but as the typical SC generation experiment does not require a very long piece of fiber, another solution is to draw the fiber in the form of a very long taper, i.e., gradually increase/decrease the fiber diameter, thus a certain part of the fiber could meet the targeted hole size.

According to the simulation results and the discussion, the proposed seven-core PCF has a great potential to obtain a visible SC spectrum because of the proper dispersion and group-velocity characteristics. In addition, the proposed seven-core PCF has a great potential to scale up the average power of SC sources for its large mode field area compared with single-core PCFs. Therefore, it has a great potential as the primary nonlinear medium for high-power visible SC generation.

4 Conclusion

We have designed a seven-core PCF optimized for high-power visible SC generation with $\sim 1\text{-}\mu\text{m}$ pulsed lasers which has a large air-filling fraction and a large effective mode field area. The designed seven-core PCF has a ZDW shorter than and near the pump wavelength and a steeper decrease at long wavelengths in the group-velocity profile, which is essential for visible SC generation. In addition, the in-phase supermode of the designed seven-core PCF has an even mode field distribution which could endure much more power and has a larger mode field area which increases the end facet damage threshold and decreases the mode field mismatch when spliced to the large mode area double cladding pigtail fiber of the pump laser. Finally, we have simulated the SC generation with the seven-core PCF and simulation results show that the seven-core PCF has great potential as the primary nonlinear medium for high-power visible SC generation.

Acknowledgments

This work was supported by the National High Technology Research and Development Program of China (863 Program) (Grant No. 2015AA021101) and the State Key Program of National Natural Science of China (Grant No. 61235008). The authors are also grateful to Dr. Zheng-gang Lian of Yangtze Optical Electronic Company Ltd. for helpful discussions on the fiber fabrication.

References

1. J. M. Dudley, G. Genty, and S. Coen, "Supercontinuum generation in photonic crystal fiber," *Rev. Mod. Phys.* **78**, 1135–1184 (2006).
2. S. Coen et al., "White-light supercontinuum generation with 60-ps pump pulses in a photonic crystal fiber," *Opt. Lett.* **26**, 1356–1358 (2001).
3. W. J. Wadsworth et al., "Supercontinuum generation in photonic crystal fibers and optical fiber tapers: a novel light source," *J. Opt. Soc. Am.* **19**, 2148–2155 (2002).
4. J. M. Dudley and J. R. Taylor, "Ten years of nonlinear optics in photonic crystal fibre," *Nat. Photonics* **3**, 85–90 (2009).
5. H. Chen et al., "Different supercontinuum generation processes in photonic crystal fibers pumped with a 1064-nm picosecond pulse," *Chin. Phys. B* **22**, 084205 (2013).
6. X. Hu et al., "High average power, strictly all-fiber supercontinuum source with good beam quality," *Opt. Lett.* **36**, 2659–2661 (2011).
7. X. Fang et al., "Multiwatt octave-spanning supercontinuum generation in multicore photonic-crystal fiber," *Opt. Lett.* **37**, 2292–2294 (2012).
8. H. Chen et al., "All-fiber-integrated high-power supercontinuum sources based on multi-core photonic crystal fibers," *IEEE J. Sel. Top. Quantum Electron.* **20**(5), 0902008 (2014).
9. D. M. Owen et al., "Excitation-resolved hyperspectral fluorescence lifetime imaging using a UV-extended supercontinuum source," *Opt. Lett.* **32**, 3408–3410 (2007).
10. S. Meissner et al., "A new small-package super-continuum light source for optical coherence tomography," *Proc. SPIE* **8611**, 86110K (2013).
11. L. Olofsson and E. Margeat, "Pulsed interleaved excitation fluorescence spectroscopy with a supercontinuum source," *Opt. Express* **21**, 3370–3378 (2013).
12. J. M. Stone and J. C. Knight, "Visibly 'white' light generation in uniform photonic crystal fiber using a microchip laser," *Opt. Express* **16**, 2670–2675 (2008).
13. N. Akhmediev and M. Karlsson, "Cherenkov radiation emitted by solitons in optical fibers," *Phys. Rev. A* **51**, 2602–2607 (1995).
14. F. M. Mitschke and L. F. Mollenauer, "Discovery of the soliton self-frequency shift," *Opt. Lett.* **11**, 659–661 (1986).
15. M. H. Frosz et al., "Increasing the blue-shift of a picosecond pumped supercontinuum," in *Supercontinuum Gener. Opt. Fibers*, J. M. Dudley, Ed., pp. 119–141, Cambridge University Press, Cambridge, UK (2010).
16. A. V. Gorbach et al., "Four-wave mixing of solitons with radiation and quasi-nondispersive wave packets at the short-wavelength edge of a supercontinuum," *Opt. Express* **14**, 9854–9863 (2006).
17. G. P. Agrawal, *Nonlinear Fiber Optics*, 4th ed., Academic Press, Singapore (2007).
18. J. Knight et al., "Anomalous dispersion in photonic crystal fiber," *IEEE Photonics Technol. Lett.* **12**, 807–809 (2000).
19. D. Ghosh et al., "Blue-extended sub-nanosecond supercontinuum generation in simply designed nonlinear microstructured optical fibers," *J. Lightwave Technol.* **29**, 146–152 (2011).
20. X. Fang et al., "Numerical analysis of mode locking in multi-core photonic crystal fiber," *Chin. Sci. Bull.* **55**, 1864–1869 (2010).
21. A. Mafi and J. V. Moloney, "Shaping modes in multicore photonic crystal fibers," *IEEE Photonics Technol. Lett.* **17**, 348–350 (2005).

Xue Qi received her MS degree in precision instrument and machinery from the Harbin Engineering University, Harbin, China, in 2010. Currently, she is working toward her PhD in optics engineering at the National University of Defense Technology, ChangSha, China. Her current research interests include active and passive mode-locked Yb-doped fiber lasers, fiber amplifiers, high-power visible supercontinuum generation, and their applications.

Biographies for the other authors are not available.